Sputter-deposited Al–Mg films – voltammetric, structural and microgravimetric characterization

Asta Grigucevičienė, Konstantinas Leinartas, Remigijus Juškėnas and Eimutis Juzeliūnas*

Institute of Chemistry, A. Goštauto 9, LT-2600 Vilnius, Lithuania

Al–Mg films with magnesium content from 0% to 98% were formed on glass and quartz substrates by magnetron sputtering technique. In order to evaluate anticorrosive resistance, the anodic behavior of the films was studied in 3.5% NaCl and 3.5% NaCl+50 ppm Cu(II) solutions. The resistance of samples increased with increase in Al content; this was evident from higher both open circuit and breakdown potentials. It has been shown that sputtered Mg–3Al, Al–4Mg and Al films had a superior resistance to corrosion when compared to their casting counterparts, which are widely used for practical applications. XRD measurements revealed a crystalline (not amorphous) structure of the sputtered deposits. The increase in magnesium content caused a change from cubic structure to hexagonal one. The grain size of sputtered samples was less than the size of casting counterparts (100–170 nm for sputter deposits and 225–300 nm for casts depending upon chemical composition). AFM images demonstrated that sputtered samples had a smoother surface than the mechanically treated alloys. The copper deposits that developed in Cu(II) solution, and the inherent domains of localized corrosion were demonstrated as well. EQCM was shown to be an informative tool to evaluate corrosion rate *in situ* for films with a relatively low content of magnesium, whereas an analogous evaluation for magnesium-rich samples was complicated by magnesium transfer to solution. The superior corrosion resistance of magnetron sputtered Al–Mg films was attributed to a higher passivation capacity of the (hydro)oxide layer developed on the sputtered deposits with reduced grain size and more uniform microstructure.

Key words: aluminium–magnesium alloys, magnetron sputtering, corrosion, AFM, EQCM

INTRODUCTION

Although the Al–Mg alloys are widely used in a variety applications (food equipment, chemical processing, aerospace and car industry, structural fields), the disadvantage of these alloys is susceptibility to pitting or exfoliation corrosion [1]. The primary reason for low corrosion resistance lies in the low protective capacity of magnesium hydroxide, which forms on the alloy surface during corrosion [1–3]. Sputter deposition may be considered as an environmentally friendly alternative to produce Al–Mg alloy films with superior resistance to corrosion. This technique has attracted considerable attention in recent years to deposit alloys with high stability in aggressive media [4–28]. The sputtered deposits, due to their chemical homogeneity and amorphous or nanocrystalline structure, may be of superior stability when compared to their crystalline counterparts. Examples are Co–Cr–Mo, Ni–Cr–Mo and Fe–Cr–Ni films [24, 26]. However, the resistance of sputtered Au–Pd–In was similar to that of the cast [25]. It has been shown by Hashimoto et al. that precipitation of nanocrystallites with dimensions less than 20 nm may increase corrosion resistance [27, 28]. Janik-Czachor et al. demonstrated that Al-refractory metal amorphous alloys exhibited a higher electrochemical passivity than crystalline aluminium [29–34].

In the present investigation, an attempt has been made to deposit by magnetron sputtering Al–Mg films with different elemental content of the both elements and to characterize the anticorrosive and structural properties of the coatings by voltammetry, XRD, AFM and EQCM. An emphasis has been made on the study of the sputtered materials, whose casting counterparts are widely used for practical purposes, *viz*., Al–4Mg, Mg–3Al and pure Al.

* Corresponding author: ejuzel@ktl.mii.lt

EXPERIMENTAL

Commercially available Al–4Mg and Mg–3Al alloys were used as sputtering targets. The Mg–3Al target (a disc 30 mm in diameter and 0.5 mm thick) was supplemented with an Al target of different size in order to vary the content of aluminium in the deposit. A rectangular gap of different dimensions (depending on a desirable Al concentration) was cut off in the Mg–3Al target and an aluminium plate of the same dimensions was mounted in the gap. Five specimens were prepared simultaneously during one sputtering procedure to provide the same content of elements in the samples. The coating thickness was *ca.* 2 μm.

The surfaces of pure aluminium and casting alloys were polished with SiC paper (grade 2500), washed with acetone and dried.

The sputtering chamber was evacuated, filled with Ar and its pressure was maintained at 0.1–0.2 Pa. The temperature in the chamber was *ca*. 50 °C. The Ar ionisation current was 60 mA and the voltage was 450 V. The sputtering duration usually was 10 min, which corresponded to a coating thickness of *ca*. 0.2–0.3 μm. To prepare thicker samples for XRD and XPS studies (1–2 μm), the duration of sputtering was extended.

The XPS spectra were recorded with an Escalab MK II spectrometer (Great Britain) using X-radiation of MgK_α (1253.6 eV, pass energy of 20 eV). To obtain depth profiles, the samples were etched in the preparation chamber by ionised argon in a 5×10^{-4} Pa vacuum. An accelerating voltage of *ca*. 15 kV and a beam current of 20 μA cm^{-2} were used, which corresponded to an etching rate of *ca*. 2 nm min^{-1}.

The exact composition of the Al–4Mg alloy according to electron probe microanalysis was as follows (in mass %): Al – 95.24, Mg – 3.74, Si – 0.38, Fe – 0.33, Mn – 0.17, Zn – 0.05, Cu – 0.03, Cr – 0.04, Pb – 0.007, Ni – 0.004, Ti – 0.011. The elemental content at a depth of 60 nm of the sputtered coating was found by XPS analysis (in mass %): Al – 93.9, Mg – 3.6, Cu – 0.49, Fe – 0.28, Zn – 0.18, Mn – 0.47, Si – 0.8. Thus, sputter-deposited coating had a similar content of Al and Mg as compared to the alloy used as a sputtering target. The analogous data for Mg–3Al target were as follows: Mg – 95.34, Al – 3.65, Cu – 0.37, Zn – 0.64. The composition of the sputtered film was: Mg – 95.8, Al – 3.15, Cu – 0.35, Zn – 0.65.

X-ray diffraction (XRD) investigations were carried out using a D8 Advance diffractometer (Bruker AXS, Germany) with CuK_α radiation selected by a secondary graphite monochromator. The step-scan mode with a step of 0.05° 2θ and a sampling time of 10 s/step in the range $30° \le 2\theta \le 70°$ was used.

The AFM measurements were conducted using a TopoMetrix Explorer SPM. The images were obtained with a Si_3N_4 tip in the contact mode.

The EQCM experimental device was analogous to that described previously [22–25]. Quartz discs with fundamental frequency f_0 = 5 MHz were used. Both sides of the quartz were coated with the alloy film and mounted in a special window of an electrochemical cell, with one side exposed to the cell compartment. The quartz discs 15 mm in diameter (AT plane) produced by KVG Quartz Crystal Technology GmbH (Germany) were used.

A saturated Ag/AgCl/KCl electrode was used as reference. A platinum foil served as a counter electrode. The voltammetric measurements were conducted by an IM6 apparatus from Zahner (Germany) using the same cell as for EQCM measurements.

Analytical grade purity NaCl and $CuCl_2$ salts and triply distilled water were used to prepare solutions. The measurements were carried out at 20 °C.

RESULTS AND DISCUSSION

Figure 1 shows the anodic potentiodynamic curves obtained in 3.5% NaCl solution for Al–Mg films and casting alloys with different elemental contents. Curve 1 is for Mg–3Al cast, whose exact composition is given in the experimental section. The curve location indicates the highest anodic activity of that specimen as compared to other systems. Curve 2 is for a sputtered Mg–3Al film, whose composition is similar to that of the cast alloy (for exact data see the experimental section). When both curves are

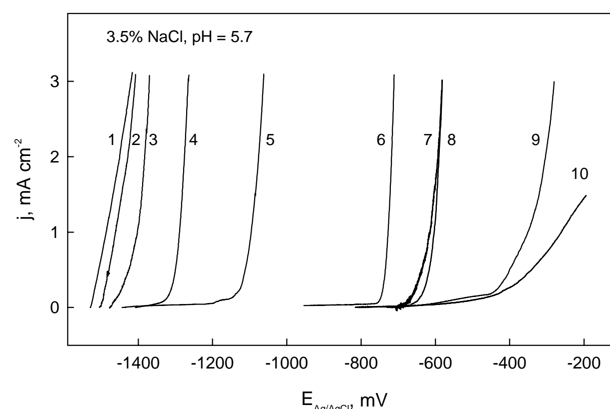

Fig. 1. Anodic potentiodynamic curves (v = 5 mV s^{-1}) obtained in 3.5% NaCl solution for cast (1, 7, 8) and sputtered (2–6, 9, 10) samples: 1 – Mg–3Al (cast), 2 – Mg–3Al, 3 – Mg–10Al, 4 – Mg–20Al, 5 – Mg–42Al, 6 – Mg–63Al, 7 – Mg–96Al (cast), 8 – Al (cast), 9 – Mg–96Al, 10 – Al

compared, one can see that the sputtered specimen is more stable than its casting counterpart.

The increase in Al content (c_{Al}) leads to a positive shift of the open circuit potential and higher electrode polarization, which indicates an increase in sample stability with an increase in c_{Al}. It is a characteristic feature that the curves for $c_{Al} \leq 10\%$ do not have a passive region, *i.e.* the films actively dissolve above the open circuit potential. By contrast, the systems with $c_{Al} \geq 10\%$ do exhibit a passive behaviour during a positive potential sweep. The stability of these alloys could be characterized by the breakdown potential value, at which the passive layer starts to be destroyed and an exponential current increase begins. The values of breakdown potentials clearly show that the stability increases when aluminium content is increased.

The voltammetric curves for the composition Al–4Mg were obtained for both sputtered and cast samples (Fig. 1, curves 7 and 9). The data clearly indicate a superior resistance of the sputtered sample, since it is characterized by a much higher breakdown potential value and lower rates of anodic dissolution.

Curves 8 and 10 in Fig. 1 are related to magnesium-free specimens. Again, the sputtered film has a higher resistance when compared to its casting counterpart. It is also evident that the sputtered Al–4Mg film is more resistant than the pure Al cast.

Thus, a conclusion may be drawn that the sputtered Mg–3Al, Al–4Mg and Al films have a superior anticorrosion stability than their casting counterparts. It is noteworthy that Al–4Mg and pure Al films showed an especially great anticorrosive effect for.

It is commonly known that heavy metals deposited on Al surface accelerate corrosion, which represents a serious technical issue [1]. Samples were studied in solution containing 50 ppm Cu(II) (Fig. 2), which represents a much more aggressive environment than the copper-free NaCl solution (Fig. 1). Figure 2 shows that in this highly corrosive environment the sputtered samples also exhibited a higher resistance. This is obvious when comparing curves 1 and 2 (Mg–3Al), 6 and 8 (Al–4Mg), 7 and 9 (Al). Thus, the conclusion about a superior anticorrosive resistance of sputtered samples has been confirmed.

Figure 3 compares XRD patterns for the sputtered specimens with different elemental content. The coatings with a high content of aluminium (c_{Al} = = 100% ÷ 96%) actually do not have a clearly pronounced texture, as can be seen from relatively small intensities of the XRD peaks. The coating with 63% of Al exhibits a <111> texture with a face-centred cubic (fcc) structure, which is typical of aluminium. When aluminium content decreases (c_{Al} = 42% ÷ 3%), the structure changes from cubic to hexagonal one with a texture <001>, which is typical of magnesium. The coatings with a high content of magnesium (c_{Al} = 3%, 10%) are strongly textured as is evident from the narrow peaks. The peaks for c_{Al} = 42% and c_{Al} = 20% are more outspread as compared to other samples. This is indicative of inhomogeneity of these samples due to the transition from a cubic structure to a hexagonal one. The similar change in structure with elemental content was observed also for other alloy systems, for instance, Ni–Fe alloy [35]. The authors came to the conclusion that the smallest grain size was typical at concentrations at which a transition from face-centred structure to a body-centred one took place.

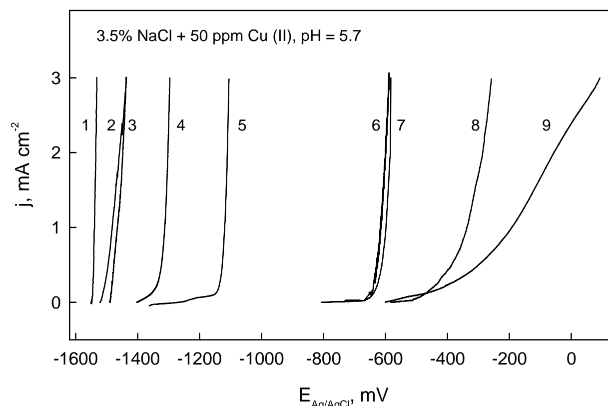

Fig. 2. Anodic potentiodynamic curves (v = 5 mV s^{-1}) obtained in 3.5% NaCl+50 ppm Cu(II) solution for cast (1, 6, 7) magnetron-sputtered (2–5, 8, 9) samples: 1 – Mg–3Al (cast), 2 – Mg–3Al, 3 – Mg–10Al, 4 – Mg–20Al, 5 – Mg–42Al, 6 – Mg–96Al (cast), 7 – Al (cast), 8– Mg–96Al, 9 – Al

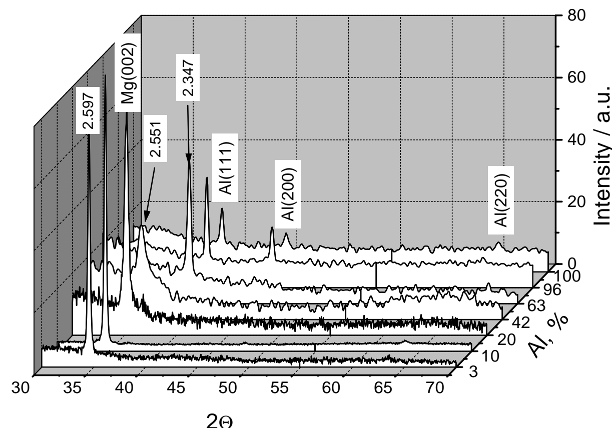

Fig. 3. XRD patterns obtained for sputtered Al–Mg films on glass substrate with different elemental content

Figures 4–6 compare the XRD data obtained for sputtered and cast samples. The sharp XRD peaks

indicate a perfect crystalline structure of all cast samples (the peaks are indexed). The Al and Al–4Mg casts have a strong <110> texture (Figs. 4, 5), while the texture <001> is predominant for Mg–3Al sample (Fig. 6). The structures of the sputtered deposits are different from those of the cast samples. So, the texture <111> is predominant for sputtered Al and Al–4Mg, whereas the analogous casts are characterized by the textures <110>, <111> and <100> of Al. It is characteristic that Al and Al–4Mg casts are more strongly textured than the sputtered deposits. By contrast, the sputtered Mg–3Al coating exhibits a more textured structure <001> than the cast.

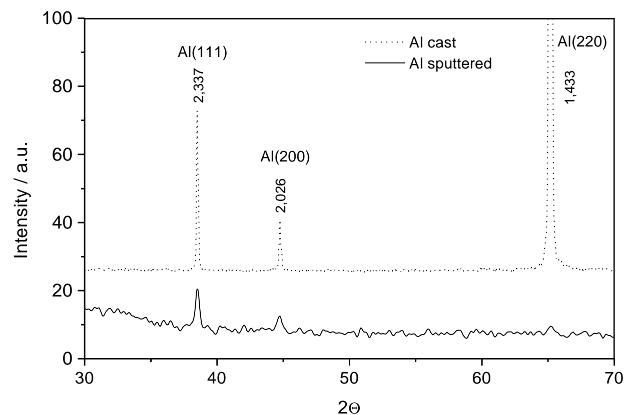

Fig. 4. XRD patterns obtained for Al cast (upper curve) and magnetron-sputtered aluminium film on glass substrate

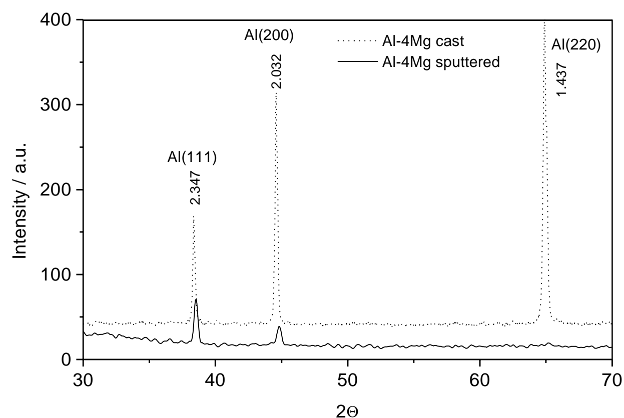

Fig. 5. XRD patterns obtained for Al–4Mg cast (upper curve) and magnetron-sputtered film of analogous composition on glass substrate

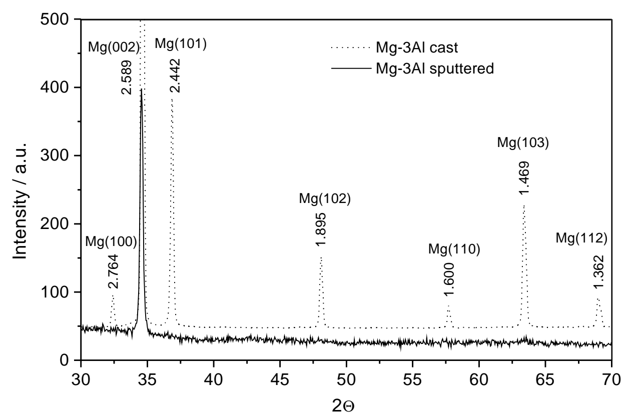

Fig. 6. XRD patterns obtained for Mg–3Al cast (upper curve) and magnetron-sputtered film of analogous composition on glass substrate

The grain size of the deposits was evaluated according to Sherrer's well-known relation:

$$D = \frac{0.9\lambda}{\beta \cos \Theta} \tag{1}$$

where D is the grain size in angströms, λ is the X-ray wavelength, which is for Cu $K_{\alpha 1}$ radiation λ = 1.54051 Å, and Θ is the diffraction angle of the peak. The β value means the outspread of the XRD peak in radians; it was calculated according to the ratio

$$\beta = B - b \tag{2}$$

with B spread at a half of the intensity, b is the analogous value for a standard (in our case for a cast alloy) with D > 200–250 nm.

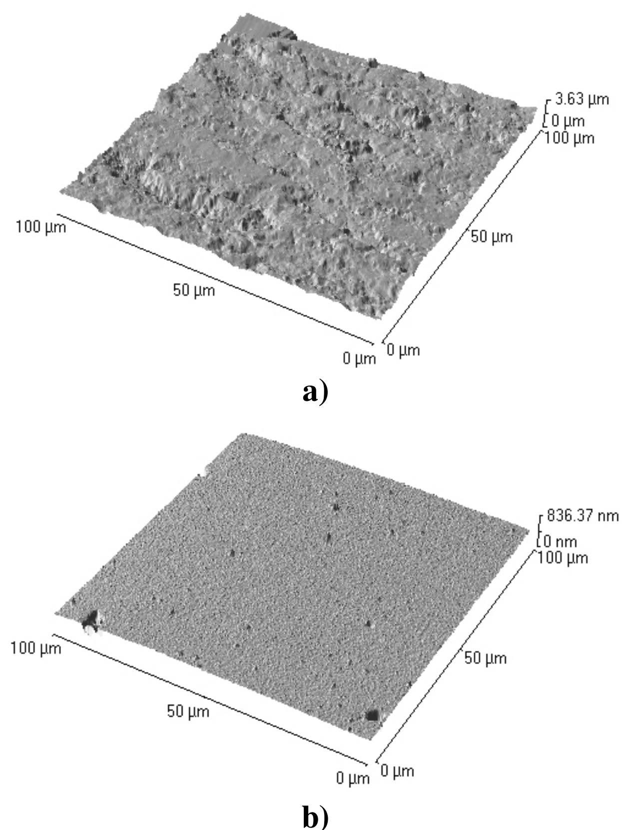

Fig. 7. AFM images of Al–4Mg cast and abraded surface (*a*) and magnetron-sputtered film on glass substrate (*b*)

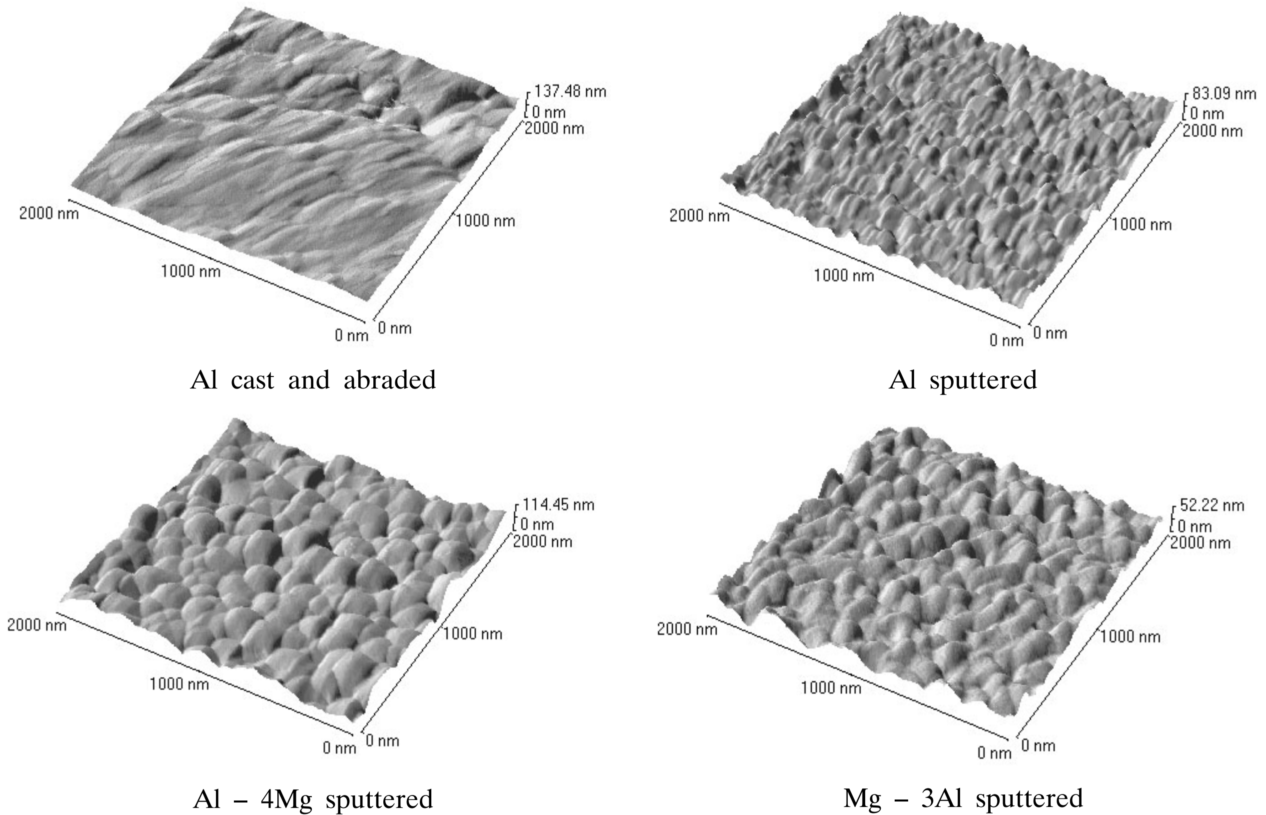

Fig. 8. AFM images of surface microstructures of Al cast and abraded and sputtered Al, Al–4Mg and Mg–3Al

The grain size for sputtered aluminum (Fig. 4) was found to be $D_{sp} \approx 100$ nm. The aluminum cast is characterized by a greater value $D_{cast} \approx 225$ nm. The analogous parameters for Al–4Mg (Fig. 5) are $D_{sp} \approx 90$ nm and $D_{cast} \approx 250$ nm. The magnesium-rich samples Mg–3Al (Fig. 6) are characterized by $D_{sp} \approx 170$ nm and $D_{cast} > 300$ nm. Thus, a conclusion may be drawn that sputtered films have a much finer crystal structure than casting materials. It is also obvious that magnesium-rich samples (both sputtered and cast) have larger grain sizes than the aluminum-rich samples.

The surface microstructures of cast and sputtered materials are demonstrated by AFM images in Figs. 7–11. Figure 7 shows that a sputtered specimen (b) on a micrometer scale has a much smoother surface than a mechanically abraded alloy (a). Figure 8 represents the micro-topography on a smaller scale, which shows the similar surface microstructure for the sputtered samples with different elemental content.

The AFM image in Fig. 9a shows copper deposits developed on the sputter deposited Al–4Mg during its exposure for 5 min to 3.5 NaCl + 50 ppm Cu(II) solution. The deposits have dimensions in order of tens of micrometers. A nobler copper deposits on a less noble Al–Mg and represent a system of micro-cathodes, on which water decomposi-

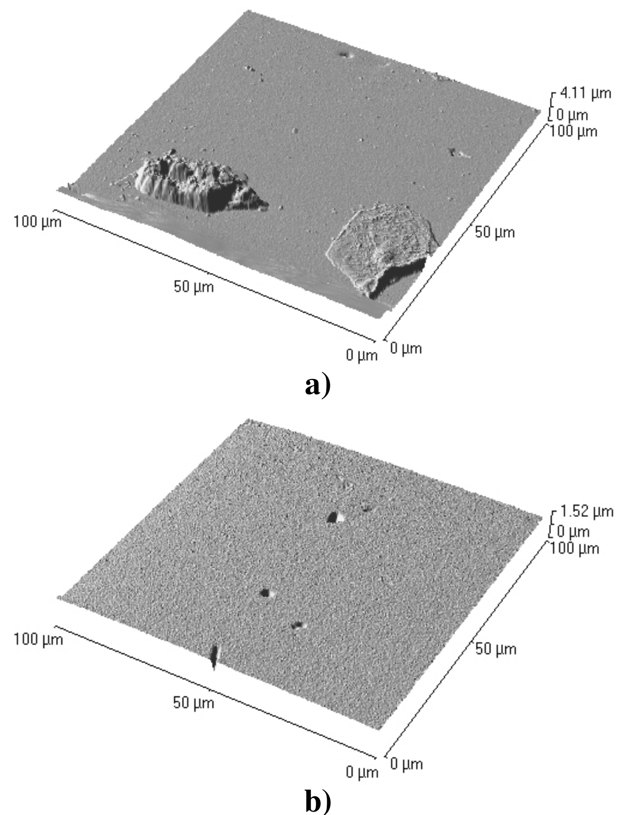

Fig. 9. AFM images of magnetron sputtered Al–4Mg surface on glass obtained after 5 min of immersion in 3.5% NaCl + 50 ppm Cu(II) (*a*) and in 3.5% NaCl solution (*b*)

tion is accelerated. It is noteworthy that copper deposits on the sputtered surface (Fig. 9a) do not differ greatly in shape and size from those on cast and abraded surfaces (10a).

Figure 11 shows typical copper deposits on a magnesium-rich sample (Mg–3Al). Interestingly, these copper deposits have a weak adhesion to the substrate. So, they have not been found on the surface either by AFM or by XPS analysis after surface washing with a water stream using a conventional laboratory rinsing balloon. The reason is that the magnesium hydroxide film (on which most probably copper deposition takes place) is weakly bound to the alloy surface as has been discussed in order to explain the low passivation capacity of the hydroxide [1–3].

The inherent domains of localized corrosion (corrosion pits), which developed during a 5-min exposure of the sputtered film to 3.5% NaCl solution, are shown in Fig. 9b. The pits have the size in the order of several microns. Figure 10b shows an analogous AFM image for a cast surface.

Figure 12 shows the mass change during the first stages of corrosion registered by EQCM after immersion of samples of different composition into 3.5% NaCl and 3.5% NaCl + 50 ppm Cu(II) solutions (*a* and *b*, respectively). The general EQCM response is a mass gain, which implies accumulation of corrosion products on the corroding surface. Clearly, the mass change for pure aluminium

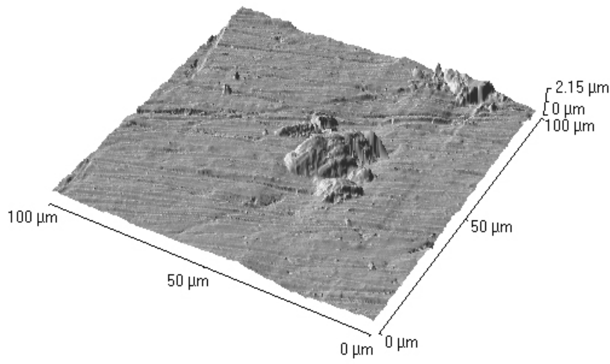

a)

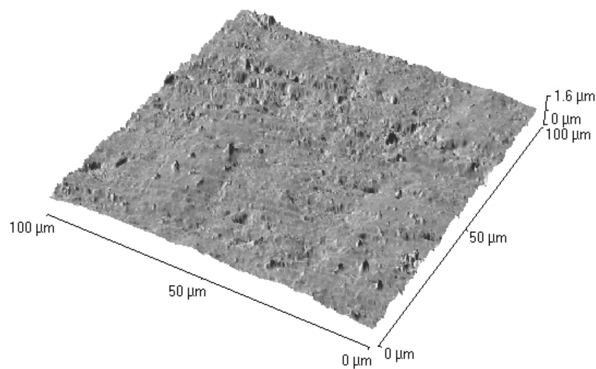

b)

Fig. 10. AFM image of cast and abraded Al–4Mg surface obtained after 5 min of immersion in 3.5% NaCl + 50 ppm Cu(II) (*a*) and in 3.5% NaCl solution (*b*)

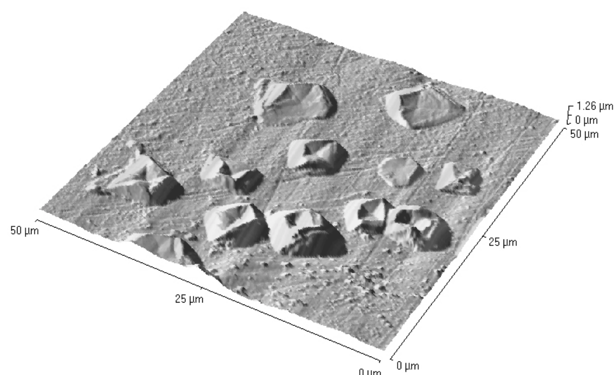

Fig. 11. AFM image of cast and abraded Mg–3Al surface obtained after 5 min of immersion in 3.5% NaCl + 50 ppm Cu(II)

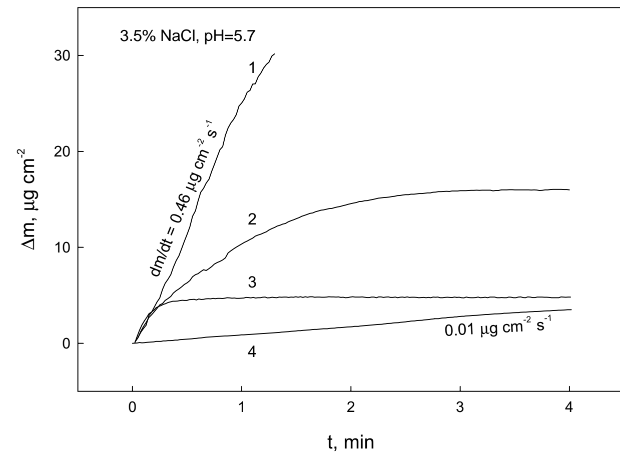

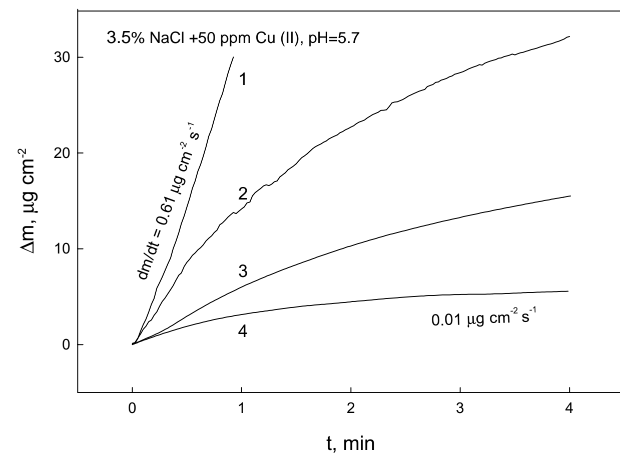

Fig. 12. Mass change of magnetron sputtered Al–Mg coatings determined by EQCM during corrosion in 3.5% NaCl (*a*) and 3.5% NaCl + 50ppm Cu(II) (*b*). Elemental content: 1– Mg–20Al, 2 – Mg–3Al, 3 – Al–4Mg, 4 – Al

(dm/dt = 0.01 μg cm^{-2} s^{-1}) is significantly less than for magnesium-containing specimens, which indicates aluminium to have a higher corrosion resistance. The average corrosion rate of Al–4Mg sample in Cu (II) environment is about twice as high as that of pure aluminium, what is evident from the total mass change after the time interval under study (4 min). A very high mass gain rate is observed for a Mg–20Al sample (dm/dt = 0.61 μg cm^{-2} s^{-1}), indicating that the sample is very susceptible to corrosion.

It is a symptomatic feature in both solutions under study that the mass gain for the magnesium-rich sample (c_{Al} = 3%) is less than the analogous rate for the sample with a higher content of aluminum (c_{Al} = 20%). This observation seems to contradict with the results of voltammetric measurements, which clearly indicate that the corrosion resistance of Mg–3Al is much higher than that of Mg–20Al (Figs. 1 and 2). The reason for this seeming contradiction lies in the fact that a significant part of magnesium corrosion products should be transferred to the solution and not accumulated on the surface of the microbalance. Magnesium corrosion may be described by anodic dissolution

$$Mg \rightarrow Mg^{2+} + 2e \quad (E° = -2.37\ V) \qquad (3)$$

and cathodic water decomposition

$$2H_2O + 2e \rightarrow H_2 + 2OH^-. \quad (E° = -0.828\ V) \qquad (4)$$

These electrochemical reactions in neutral solutions may be accompanied by hydroxide precipitation:

$$Mg^{2+} + 2(OH)^- \rightarrow Mg\ (OH)_2. \qquad (5)$$

However, let us remember that the solubility of $Mg(OH)_2$ in water at 18 °C is 0.09 g l^{-1} [36] and the hydroxide is weakly bound to the surface, as is discussed above. So, the magnesium content, which is not accumulated on the corroding surface, should be estimated in order to calculate the corrosion rate from EQCM data. By contrast, aluminum corrosion product

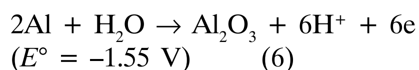

$$2Al + H_2O \rightarrow Al_2O_3 + 6H^+ + 6e \quad (E° = -1.55\ V) \qquad (6)$$

is accumulated on the surface due to its very low solubility and strong adhesion to the metal surface.

Thus, while the microgravimetric approach is an effective tool for evaluating the corrosion resistance of aluminum-rich samples, this seems to be more problematic procedure in the case of samples with a higher magnesium content.

It has been shown previously that EQCM measurements can be effectively applied to evaluate corrosion resistance of sputter-deposited materials. So, the corrosion dynamics of magnetron sputtered films (Al–Mg, Au–Pd–In, Co–Cr–Mo, Ni–Cr–Mo, Fe–Cr–Ni, Fe–Cr–Ni–Ta) were studied in different liquid and gaseous media and the quantitative approach to corrosion resistance evaluation has been demonstrated [21–26, 37].

The presented data have shown that magnetron-sputtered Al–Mg coatings have superior anticorrosive properties when compared to those of their casting counterparts. The main reason for the increased resistance should lie in a higher passivation capacity of the (hydro)oxide films formed on the sputtered surfaces with a smaller grain size and more uniform surface-microstructure. As a result, one can expect that passive layers on the sputtered surfaces will contain less defects and weak sites. Some previous observations support this assumption. We have found that the anticorrosive superiority of sputtered coatings was pronounced only under the conditions when even passive film stability was a key factor in overall corrosive behaviour. For instance, the superior resistance of sputtered Fe–Cr–Ni was evident only in chloride solutions, while in sulphate ones this difference was negligible [38]. The effect was attributed to a superior stability of passive layers against the chloride, which has a higher disintegration capability than the sulphate. In this paper, we have also shown that a great anticorrosive effect is observed for sputtered aluminium or aluminium-rich samples, *i.e.* for those forming stable passive films. The effect was rather weak for the magnesium-rich sample, because the passivation capacity of magnesium film is typically low.

As a concluding remark, it should be noted that the magnetron-sputtered Al–Mg alloy films due to their high anticorrosive resistance seem promising for practical applications. For instance, these coatings may be used to protect Al–Mg cast alloys susceptible to corrosion, provided good adhesion between the substrate (oxidized alloy surface) and the coating is ensured. Such corrosion-resistant coatings may be considered as an environmentally friendly alternative to chromate conversion coatings, whose application tends to be problematic due to the environmental regulations. In general, the widespread application of sputter-deposited coatings is limited for the meantime by their expensiveness, and future efforts should be addressed to search for competitive sputtering technologies.

CONCLUSIONS

Measurements of anodic activity and breakdown potentials indicated a superior corrosion resistance of

magnetron-sputtered Al–Mg coatings with respect to their cast counterparts.

The XPS depth profile analysis has shown that the chemical composition of the magnetron-sputtered Al–Mg deposits is similar to that of the cast alloy used as a magnetron-sputtering target.

The aluminium-rich coatings (Al, Al–4Mg) have a cubic structure with a pronounced <111> texture of aluminium. When the aluminium content decreased (42÷3Al), the structure changed from cubic to hexagonal with a texture <001>, which is typical of magnesium.

The structure of the sputtered deposits differed from that of the cast alloys. For instance, the texture <111> was characteristic of the sputtered Al and Al–4Mg samples, whereas the cast counterparts were characterized by the textures <110>, <111> and <100> of Al.

The grain size of sputtered materials was less than the size of the casts: $D_{sp} \approx 100$ nm and $D_{cast} \approx$ ≈ 225 nm for Al, $D_{sp} \approx 90$ nm and $D_{cast} \approx 250$ nm for Al–4Mg and $D_{sp} \approx 170$ nm and $D_{cast} > 300$ nm for Mg–3Al.

AFM images have demonstrated on a micrometer scale that the sputtered deposits have a much smoother surface than the mechanically abraded alloys. The deposits developed in Cu(II) environment on both cast and sputtered surfaces have dimensions in the order of tens of micrometers.

Microgravimetric measurements are an informative approach, which provides sensitive corrosion data *in situ* on Al–Mg coatings with a relatively low content of magnesium. The study of magnesium-rich coatings is complicated by magnesium transfer to solution.

Acknowledgements. The assistance of V. Lisauskas and A. Sudavičius in magnetron sputtering and XPS analysis is greatly acknowledged.

Received 19 September 2003
Accepted 18 November 2003

References

1. D. A. Jones, Principles and Prevention of Corrosion, Prentice-Hall, Inc. Upper Saddle River, NJ 07458 (1996).
2. E. Brillas, P. L. Cabot, F. Centellas, J. A. Garrido, E. Perez and R. M. Rodriguez, *Electrochim. Acta,* **43**, 799 (1998).
3. J. H. Nordlien, K. Nisancioglu, S. Ono and N. Masuko, *J. Electrochem. Soc.,* **143**, 2564 (1996).
4. X.-Y. Li, E. Akiyama, H. Habazaki, A. Kawashima, K. Asami and K. Hashimoto, *Corros. Sci.,* **41**, 1849 (1999).
5. H. Habazaki, K. Shimizu, P. Skeldon, G. E. Thompson and G. C. Wood, *Corros. Sci.,* **43**, 1393 (2001).
6. H. Habazaki, K. Shimizu, P. Skeldon, G. E. Thompson and G. C. Wood, *Thin Solid Films,* **300**, 131 (1997).
7. H. Habazaki, K. Takahiro, S. Yamaguchi, K. Shimizu, P. Skeldon, G. E. Thompson and G. C. Wood, *J. Electrochem. Soc.,* **146**, 2502 (1999).
8. H. Habazaki, P. Skeldon, G. E. Thompson, G. C. Wood and K. Shimizu, *J. Mater. Res.,* **12**, 1885 (1997).
9. H. Habazaki, K. Shimizu, P. Skeldon, G. E. Thompson and G. C. Wood, *Corros. Sci.,* **39**, 731 (1997).
10. H. Habazaki, P. Skeldon, G. E. Thompson, J. Wan, G. C. Wood, X. Zhou, J. Delaet and K. Shimizu, *J. Electrochem. Soc.,* **144**, 4217 (1997).
11. M. P. Ryan, N. J. Laycock, H. S. Isaacs and R. C. Newman, *J. Electrochem. Soc.,* **146**, 91 (1999).
12. Z. Y. Liu, W. Gao, K. L. Dahm and F. H. Wang, *Acta Materialia,* **46**, 1691 (1998).
13. D. Landolt, C. Robyr and P. Mettraux, *Corrosion,* **54**, 772 (1998).
14. P. Schmutz and D. Landolt, *Corros. Sci.,* **41**, 2143 (1999).
15. J. C. Oliveira, A. Cavaleiro and C. M. A. Brett, *Corros. Sci.,* **42**, 1881 (2000).
16. M. Yamasaki, H. Habazaki, K. Asami and K. Hashimoto, *J. Electrochem. Soc.,* **147**, 4502 (2000).
17. H. Mitsui, H. Habazaki, K. Asami, K. Hashimoto and S. Mrowec, *Corros. Sci.,* **38**, 1431 (1996).
18. M. Mehmood, E. Akiyama, H. Habazaki, A. Kawashima, K. Asami and K. Hashimoto, *Corros. Sci.,* **41**, 1871 (1999).
19. J. Bhattarai, E. Akiyama, H. Habazaki, A. Kawashima, K. Asami and K. Hashimoto, *Corros. Sci.,* **40**, 19 (1998).
20. J. Bhattarai, E. Akiyama, H. Habazaki, A. Kawashima, K. Asami and K. Hashimoto, *Corros. Sci.,* **40**, 155 (1998).
21. E. Juzeliūnas, K. Leinartas, M. Samulevičienė, D. Jelinskienė, A. Sudavičius, P. Miečinskas, V. Lisauskas and B. Vengalis, In: ICCE/7 (Seventh Annual International Conference on Composites Engineering), Denver, Colorado, USA, (2000) 405.
22. K. Leinartas, M. Samulevičienė, A. Bagdonas, A. Sudavičius, V. Lisauskas and E. Juzeliūnas, *Electrochem. Commun,* **3**, 494 (2001).
23. K. Leinartas, P. Miečinskas, A. Sudavičius, D. Jelinskienė, R. Juškėnas, V. Lisauskas, B. Vengalis and E. Juzeliūnas, *J. Appl. Electrochem.,* **31**(10) 1079 (2001).
24. E. Juzeliūnas, K. Leinartas, M. Samulevičienė, A. Sudavičius, P. Miečinskas, R. Juškėnas and V. Lisauskas, *J. Solid State Electrochem.,* **6**, 302 (2002).
25. E. Juzeliūnas, K. Leinartas, M. Samulevičienė, P. Miečinskas, R. Juškėnas and A. Sudavičius, *Corros. Sci.,* **44**, 1541 (2002).
26. K. Leinartas, M. Samulevičienė, A. Bagdonas, A. Sudavičius, V. Lisauskas and E. Juzeliūnas, *Chemija,* **13**, 41 (2002).
27. M. Mehmood, E. Akiyama, H. Habazaki, A. Kawashima, K. Asami and K. Hashimoto, *Corros. Sci.,* **40**, 1 (1998).
28. M. Mehmood, E. Akiyama, H. Habazaki, A. Kawashima, K. Asami and K. Hashimoto, *Corros. Sci.,* **41**, 477 (1999).

29. M. Janik-Czachor, A. Wolowik and Z. Werner, *Corros. Sci.,* **36**, 1921 (1994).
30. A. Wolowik, M. Janik-Czachor and Z. Werner, *Mat. Sci. Eng. Suppl.,* **226–228**, 398 (1997).
31. A. Wolowik, M. Janik-Czachor and Z. Werner, *Mat. Chem. Phys*., **49**, 164 (1997).
32. M. Janik-Czachor, A. Wolowik, A. Szummer, K. Lublinska, S. Hofmann and K. Kraus, *Electrochim. Acta,* **43**, 875 (1998).
33. A. Wolowik, M. Janik-Czachor, Z. Werner, G. C. Wood, G. E. Thompson, P. Skeldon, J. R. Walton and X. Zhou, *Corros. Sci.,* **40**, 731 (1998).
34. A. Wolowik and M. Janik-Czachor, *Mat. Sci. Eng.,* A267, 301 (1999).
35. N. V. Myung and K. Nobe, *J. Electrochem. Soc.,* **148**, C136 (2001).
36. Handbook of Chemistry and Physics, Ed. D. R. Lide, 73rd edition, 1992–1993.
37. V. Uksiene, K. Leinartas, R. Juskenas, A. Sudavicius and E. Juzeliunas, *Electrochem. Commun.,* **4**, 747 (2002).
38. K. Leinartas, M. Samuleviciene, A. Bagdonas, R. Juskenas and E. Juzeliunas, *Surf. Coat. Technol.,* **168**, 70 (2003).

A. Grigucevičienė, K. Leinartas, R. Juškėnas, E. Juzeliūnas

MAGNETRONINIAI AL–MG LYDINIAI – VOLTAMMETRINIS, STRUKTŪRINIS, MIKROGRAVIMETRINIS APIBŪDINIMAS

S a n t r a u k a

Įvairios sudėties Al–Mg lydiniai buvo suformuoti magnetroninio dulkinimo būdu ant stiklo ir kvarco padėklų. Lydinių antikorozinis atsparumas buvo įvertintas voltamperometriniu ir EKKM metodais 3,5% NaCl ir 3,5% NaCl+50 ppm Cu(II) tirpaluose. Nustatyta, kad korozinis atsparumas didėja didinant Al koncentraciją lydinyje. Lydinių su didele Mg koncentracija mikrogravimetrijos duomenų interpretacija komplikuota dėl intensyvaus tirpimo. Magnetroniu būdu pagaminti Mg–3Al, Al–4Mg lydiniai ir Al yra gerokai atsparesni korozijai nei jų metalurginiai analogai. Rentgeno difrakcijos ir atominės jėgos mikroskopijos metodais nustatyta, kad magnetroniai lydiniai apibūdinami mažesniais kristalų dydžiais bei tolygesne mikrostruktūra. Šie veiksniai sąlygoja atsparesnio pasyvacinio sluoksnio susidarymą paviršiuje. Cu(II) tirpale lydinių paviršiuje susiformuoja specifinės formos metalinio vario dariniai, skatinantys koroziją.